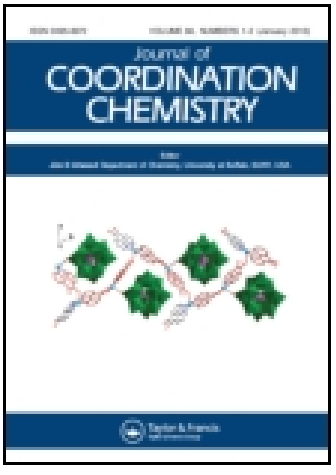

Journal of Coordination Chemistry
Publication details, including instructions for authors and subscription information:
http://www.tandfonline.com/loi/gcoo20

2-(2-Hydroxy-4-methoxybenzoyl)benzoic acid derivatives of Group 4 metal alkoxides

Timothy J. Boyle[a], Daniel T. Yonemoto[a], Michael L. Neville[a] & Samuel P. Bingham[a]

[a] Sandia National Laboratories, Advanced Materials Laboratory, Albuquerque, NM, USA

Accepted author version posted online: 24 Mar 2014.Published online: 15 Apr 2014.

Journal of Coordination Chemistry, 2014
Vol. 67, No. 5, 747–765, http://dx.doi.org/10.1080/00958972.2014.905684

2-(2-Hydroxy-4-methoxybenzoyl)benzoic acid derivatives of Group 4 metal alkoxides

TIMOTHY J. BOYLE*, DANIEL T. YONEMOTO, MICHAEL L. NEVILLE and SAMUEL P. BINGHAM

Sandia National Laboratories, Advanced Materials Laboratory, Albuquerque, NM, USA

(*Received 7 August 2013; accepted 26 February 2014*)

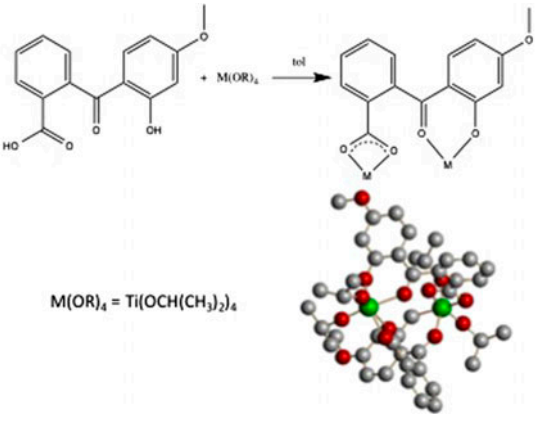

Continued exploration of the coordination behavior of derivatives of 2-benzophenone-based ligands with metal alkoxides ([$M(OR)_4$]) was undertaken from the reaction of 2-(2-hydroxy-4-methoxybenzoyl)benzoic acid (H_2-OBzA) with a series of Group 4 precursors. The products of these reactions were identified as: $[(OR)_2Ti(\mu\text{-}(c,c\text{-}OBzA))]_2$ (OR = $OCHMe_2$ (OPr^i; **1** •2tol); $OCMe_3$ (OBu^t; **2** •THF); OCH_2CMe_3 (ONep; **3**)), $[[(OPr^i)_3Ti(\mu\text{-}OPr^i)Ti(OPr^i)_2]_2(\mu\text{-}(\mu_c,\mu\text{-}OBzA))_2]_2$ (**4**), $[(ONep)_3Zr(\mu\text{-}ONep)_2Zr(ONep)_2]_2(\mu\text{-}(c,\mu\text{-}OBzA)_2)$ (**5** •tol), $[(py)(OBu^t)_3Zr]_2(\mu\text{-}(c,c\text{-}OBzA))$ (**6**), $[(OBu^t)_2Hf(\mu\text{-}OBu^t)]_2(\mu\text{-}(c,\eta^1\text{-}OBzA))$ (**7**) where 'c' = chelating or η^2; 'μ' = bridging or $\eta^1,\eta^1(O,O')$; and μ_c = bridging chelating or $\eta^1,\eta^1(O,O')$; $\eta^2:\eta^1$. The metal centers for each of these compounds adopt a pseudo-octahedral geometry employing the OBzA ligand in numerous binding modes. The different functional oxygens (carboxylate, hydroxyl, and carbonyl) were employed in a variety of coordination modes for **1**–**7**. The complexity of these OBzA-modified compounds is driven by a combination of the coordination behavior of the OBzA moieties, the size of the metal cation, and the pendant chain of the OR ligand. Solution NMR indicates a complex structure exists in solution that was considered to be consistent with the solid-state structure.

Keywords: Aroylbenzoic acid; Benzoylbenzoic acid; 2-Benzophenone; Metal alkoxide; Group 4

*Corresponding author. Email: tjboyle@Sandia.gov

1. Introduction

Metal alkoxides ([$M(OR)_x$]) have found widespread utility as precursors to ceramic oxide materials due to a number of inherent, attractive characteristics such as high solubility, low thermal decomposition, and clean conversion to the oxide (i.e. low C retention) to mention a few [1–6]. It has been demonstrated that the ligand set of [$M(OR)_x$] greatly influences the final ceramic properties by altering the precursor's central, building block core as well as the hydrolysis and condensation rates [1–6]. Therefore, the synthesis of [$M(OR)_x$] with specified structure types is of continued interest. Recently, we investigated the utility of polydentate phenols as a means to synthesize controlled, complex [$M(OR)_x$] compounds. In particular, we have been interested in exploring the effect that linked phenol ligands, such as 4,4′-methylenebis(2,6-di-*tert*-butylphenol) (H_2-4DBP), [7] and the 2-benzophenone derivatives, like 4,4′-di-methoxy,2,2′-di-ol-benzophenone (H_2-OBzP), [8] have on the final structures. These ligands were selected based on the location of the –OH reactive group and the rigidity of the ligand's backbone due to the aryl groups. The 4DBP ligand was successful in generating disubstituted species such as the simple [$(OR)_3M]_2$(μ-4DBP) [7], whereas the OBzP derivative formed more complex, interlinked species, [$(OR)_2M$(μ(c-OBzP))$]_2$ (μ – bridging (η^1, η^1) and c – chelating (η^2)).

While both ligands could generate the homometallic species, neither successfully generated mixed Group 4 species. It was reasoned that the homoleptic species preferentially formed due to increased acidity of the remaining –OH proton after the initial substitution by the most reactive [$M(OR)_x$] [9]. Any subsequent reactivity would then greatly favor a reaction with the same metal. Therefore, mixed functionalized 2-benzophenone derivatives were of interest since they could alter the reaction pathway by favoring the metathesis of one metal at one site. This led us to investigate the 2-(2-hydroxy-4-methoxybenzoyl)benzoic acid (referred to as H_2-OBzA).

The OBzA ligand maintains the rigid backbone of the OBzP species but also possesses the desired dual functional groups (–OH and HO_2C–) that are located adjacent to each other. This arrangement lends itself to numerous potential binding modes, some of which are shown in figure 1. With the dual functionality, preferential reactivity at one site *versus* another may allow for step-wise mixed metal synthesis. However, a search of the literature indicates no structural work was previously available concerning the behavior of the OBzP ligand in the presence of any transition metals [10]. Therefore, the first step prior to exploration of the production of mixed metal species was to determine the coordination behavior of OBzP in the presence of a single metal. A schematic of some of the possible binding modes of the OBzA ligands are shown in figure 1(a)–(f). The Group 4 metals were selected due to their widespread use in a variety of applications. The reaction of [$M(OR)_4$] with H_2-OBzA (equation (1)) led to the isolation of [$(OR)_2$Ti(μ-(c,c-OBzA))$]_2$ (schematic in figure 1(d): OR = $OCHMe_2$ (OPr^i; **1** •2tol: figure 2); $OCMe_3$ (OBu^t; **2**•THF: figure 3); OCH_2CMe_3 (ONep, **3**: figure 4)), [[$(OPr^i)_3$Ti(μ-OPr^i)Ti(OPr^i)$_2$]$_2$(μ-(μ_c,μ-OBzA))$_2$]$_2$ [**4**: figures 1(f) and 5], [$(ONep)_3$Zr(μ-ONep)$_2$Zr$(ONep)_2]_2$(μ-(c,μ-OBzA))$_2$ [**5** •tol: figures 1(e) and 6], [(py)$(OBu^t)_3$Zr]$_2$(μ-(c,c-OBzA)) [**6**: figures 1(d) and 7], [$(OBu^t)_2$Hf(μ-OBu^t)]$_2$ (μ-(c,η^1-OBzA)) [**7**: figures 1(c) and 8] where 'c' = chelating or η^2; 'μ' = bridging or η^1,η^1(O,O'); and μ_c = bridging chelating or η^1,η^1(O,O'); $\eta^2:\eta^1$. The synthesis and structural details of these compounds are discussed in detail.

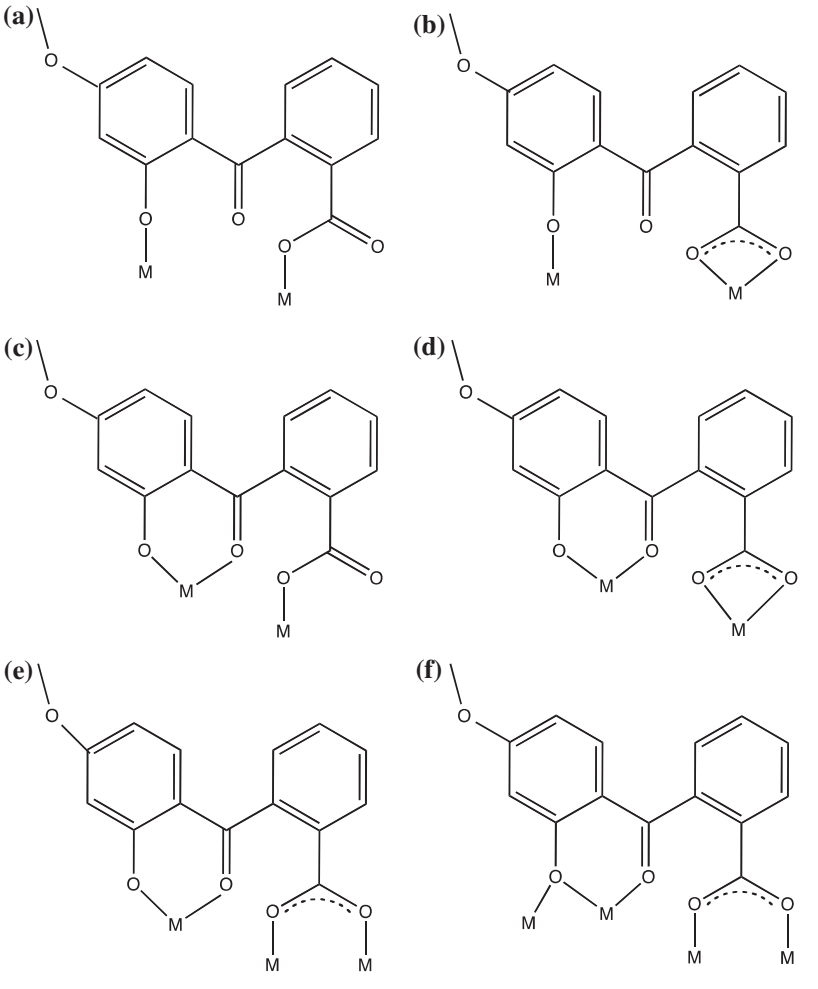

Figure 1. Schematic drawing of potential binding modes of OBzA : (a) μ-(η^1, η^1)OBzA, (b) μ-(η^1, c)OBzA, (c) μ-(c, η^1)OBzA (observed for **7**), (d) μ-(c, c)OBzA (observed for **1**, **2**, **3**, and **6**), (e) μ-(c, μ)OBzA (observed for **5**), and (f) μ-(μ_c, μ)OBzA (observed for **4**) where 'c' = chelating or η^2; 'μ' = bridging or η^1, η^1(O, O′); and μ_c = bridging chelating or μ, $\eta^2 : \eta^1$.

$$2\left[\mathrm{M(OR)_4}\right] + n\mathrm{H_2\text{-}OBzA} \rightarrow \left\{\left[(\mathrm{OR})_3\mathrm{M}\right]_2(\mu\text{-OBzA})\right\}_n + 2n\,\mathrm{HOR} \quad n = 1 \text{ or } 2; \mathrm{M} = \mathrm{Ti, Zr, Hf}. \tag{1}$$

2. Experimental

All compounds described below were handled with rigorous exclusion of air and water using standard Schlenk line and glove box techniques, unless otherwise noted. Analytical data were collected on freshly dried crystalline samples. All anhydrous solvents and precursors were used as received (from Aldrich and Alfa Aesar) without purification, including toluene, THF, py, H_2-OBzA, and $[M(OR)_4]$ (M = Ti, Zr, Hf; OR = OPr^i and/or OBu^t).

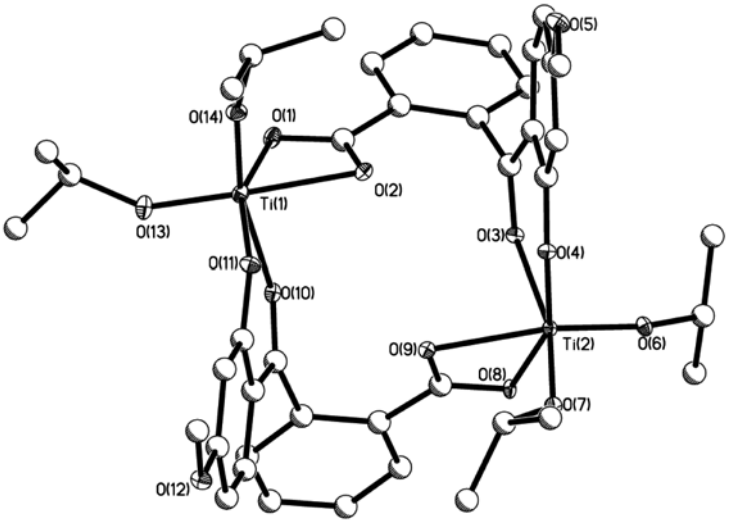

Figure 2. Structure plot of **1** •2tol. Thermal ellipsoids of heavy atoms are drawn at the 50% level and carbons are shown as stick and ball for clarity. Two *iso*-structural molecules were solved in the unit cell but only a single molecule is shown.

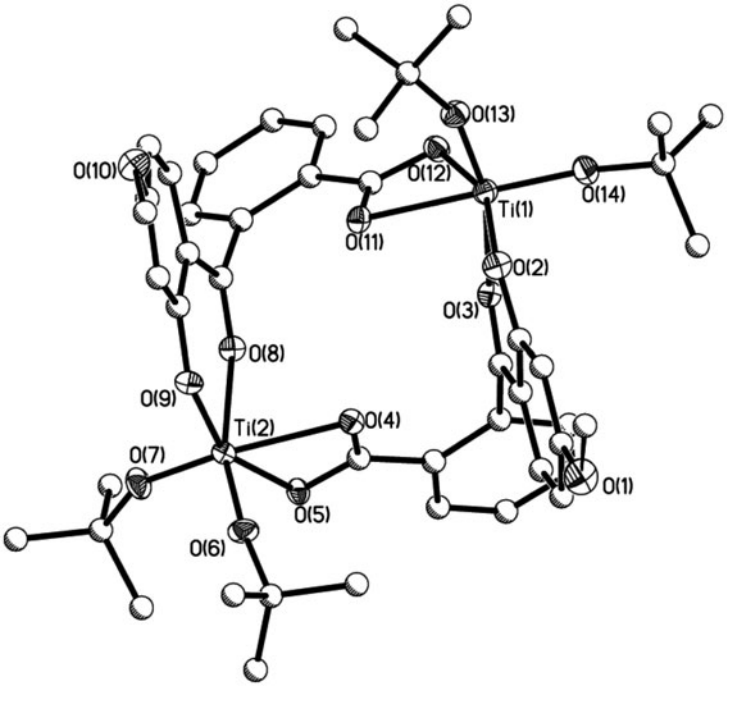

Figure 3. Structure plot of **2** •THF. Thermal ellipsoids of heavy atoms are drawn at the 50% level and carbons are shown as stick and ball for clarity. Two *iso*-structural molecules were solved in the unit cell but only a single molecule is shown.

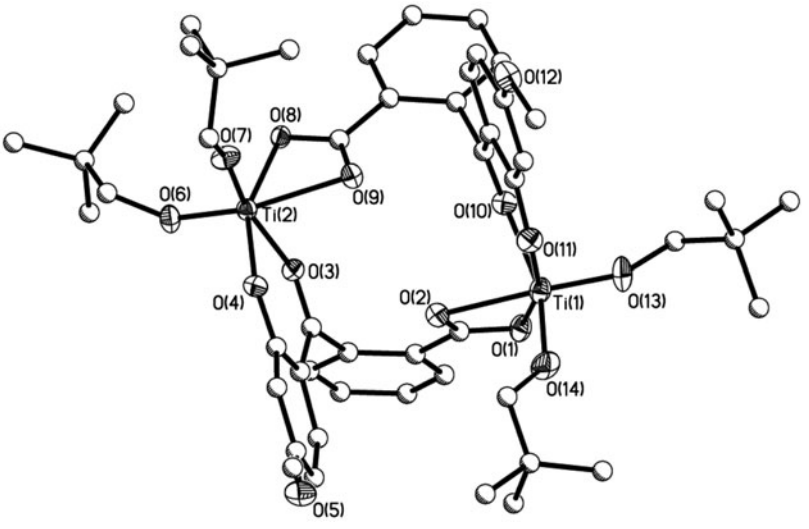

Figure 4. Structure plot of **3**. Thermal ellipsoids of heavy atoms are drawn at the 50% level and carbons are shown as stick and ball for clarity.

$[(ONep)_3Ti(\mu\text{-}ONep]_2$ [11] and $[H][(OBu^t)(ONep)_5Zr_2(\mu\text{-}ONep)_3]$ [12] (referred to as $[Ti(ONep)_4]$ and $[Zr(ONep)_4]$, respectively) were synthesized according to literature reports.

Crystalline materials that were dried *in vacuo* were used for all analytical analyses. FTIR data were collected on a Nicolet 6700 FTIR spectrometer using a KBr pellet press under a flowing atmosphere of nitrogen. Elemental analyses were collected on a Perkin Elmer 2400 Series II CHNS/O Analyzer, with samples prepared in an argon-filled glove box. All NMR samples were prepared using crystalline material handled under an argon atmosphere and made at as high a concentration as possible in the appropriate deuterated solvent and then flame-sealed under vacuum. Spectra were collected on a Bruker Avance 500 NMR spectrometer under standard experimental conditions: ^1H analysis was performed with a 4 s recycle delay at 16 scans; spectra were referenced to the toluene-d_8 peak at 2.09 ppm.

2.1. *General reaction*

In a vial in an inert atmosphere glove box, H_2-OBzA was added to a stirring, clear solution of $[M(OR)_4]$ dissolved in ~5 mL of toluene. The reaction immediately turned yellow, was stirred for 12 h, and then set aside with the cap removed to grow crystals. After the volatile component had evaporated and crystals formed, samples were removed for single-crystal X-ray analysis. For the remaining product, the mother liquor was decanted, crystals dried *in vacuo*, and the resulting yellow powders used for the remaining analyses. Yields reported are for the first crystalline batch and were not optimized.

2.2. *$[(OPr^i)_2Ti(\mu\text{-}(c,c\text{-}OBzA))]_2$ (1) •2tol*

Used $[Ti(OPr^i)_4]$ (1.00 g, 3.52 mM), H_2-OBzA (0.958 g, 3.52 mM), and toluene (~5 mL). Yield 77.8% (1.19 g). FTIR (KBr, cm^{-1}) 3067(w), 2969(m), 2930(w), 2866(w), 2622(w), 1591(s), 1522(s), 1447(m), 1420(m), 1371(s), 1331(w), 1253(m), 1215(m), 1164(m),

1121(s), 1090(w), 1020(m), 980(m), 929(w), 870(w), 854(w), 814(w), 780(w), 767(w), 732 (m), 664(w), 633(m), 606(m), 487(w), 467(w). ^{1}H NMR (500.1 MHz, tol-d_8) d 8.16 (1H, OBzA d, $J_{H\text{-}H}$ = 3.9 Hz), 7.05–7.03 (2H, OBzA, mult), 6.96 (1H, OBzA, t, $J_{H\text{-}H}$ = 7.5 Hz), 6.88 (1H, OBzA, t, $J_{H\text{-}H}$ = 7.6 Hz), 6.12 (1H, OBzA, d, $J_{H\text{-}H}$ = 4.5 Hz), 5.91 (1H, OBzA, s), 5.08 (1H, OC*H*$(CH_3)_2$, sept, $J_{H\text{-}H}$ = 6.1 Hz), 4.81 (1H, OC*H*$(CH_3)_2$, sept, $J_{H\text{-}H}$ = 6.1 Hz), 2.98 (3H, OBzA, s), 1.38, (3H, OCH(C*H*$_3)_2$, d, $J_{H\text{-}H}$ = 6.1 Hz), 1.34 (3H, OCH(C*H*$_3)_2$, d, $J_{H\text{-}H}$ = 6.1 Hz), 1.27(3H, OCH(C*H*$_3)_2$, d, $J_{H\text{-}H}$ = 6.1 Hz), 1.19 (3H, OCH(C*H*$_3)_2$, d, $J_{H\text{-}H}$ = 6.1 Hz). Anal. Calcd for $C_{42}H_{48}O_{14}Ti_2$ (%): C, 57.81; H, 5.54. Found: C, 57.55; H, 4.99.

2.3. *[(OBu^t)$_2$Ti(μ-(c,c-OBzA))]$_2$ (2) •THF*

Used [Ti(OBu^t)$_4$] (0.190 g, 0.558 mM), H_2-OBzA (0.153 g, 0.558 mM), and toluene (~10 mL). The reaction was then dried *in vacuo*, redissolved in THF, and crystals grown by slow evaporation. Yield 74.9% (0.194 g). FTIR (KBr, cm^{-1}) 3064(w), 2971(s), 2928(m), 2866 (w), 1675(m), 1593(s), 1553(s), 1516(m), 1489(m), 1460(w), 1440(w), 1378(s), 1360(s), 1319(m), 1254(m), 1223(s), 1199(s), 1130(m), 1090(w), 1027(s), 1002(s), 921(m), 892(m), 855(w), 843(w), 814(w), 776(m), 764(m), 728(m), 712(w), 660(w), 635(w), 623(w), 607 (w), 594(w), 534(w), 487(m). ^{1}H NMR (500.1 MHz, tol-d_8) d 8.14 (1H, OBzA d, $J_{H\text{-}H}$ = 2.5 Hz), 7.16 (1H, OBzA, d, $J_{H\text{-}H}$ = 2.5 Hz), 6.87 (1H, OBzA, t, $J_{H\text{-}H}$ = 7.2 Hz), 6.16 (1H, OBzA, d, $J_{H\text{-}H}$ = 4.2 Hz), 5.92 (1H, OBzA, s), 2.96 (3H, OBzA, s), 1.49, (11H, OC(C*H*$_3)_2$, s), 1.38 (10H, OC(C*H*$_3)_3$, s). Anal. Calcd for $C_{46}H_{56}O_{14}Ti_2$ (%): C, 59.49; H, 6.08. Found: C, 59.64; H, 6.55.

2.4. *[(ONep)$_2$Ti(μ-(c,c-OBzA))]$_2$ (3)*

Used [Ti(ONep)$_4$] (1.00 g, 2.53 mM), H_2-OBzA (0.687 g, 2.53 mM), and toluene (~5 mL). Yield 39.1% (0.485 g). FTIR (KBr, cm^{-1}) 2953(s), 2904(m), 2866(m), 2844(m), 1592(s), 1521(s), 1500(m), 1421(s), 1398(m), 1374(s), 1339(w), 1259(s), 1216(s), 1171(m), 1122(s), 1090(s), 1024(s), 980(w), 930(w), 870(m), 843(w), 814(w), 780(m), 767(w), 733(m), 696 (m), 666(m), 630(w), 604(m), 539(w), 478(w). ^{1}H NMR (500.1 MHz, tol-d_8) d 8.16 (1H, OBzA, d, $J_{H\text{-}H}$ = 3.9 Hz), 7.11–7.07 (2H, OBzA, mult), 6.97 (1H, OBzA, t, $J_{H\text{-}H}$ = 7.6 Hz), 6.86 (1H, OBzA, t, $J_{H\text{-}H}$ = 7.6 Hz), 6.18 (1H, OBzA, d, $J_{H\text{-}H}$ = 4.5 Hz), 5.91 (1H, OBzA, s), 4.52 (1H, OC*H*$_2$C(CH$_3)_3$, d, $J_{H\text{-}H}$ = 5.4 Hz), 4.40 (1H, OC*H*$_2$C(CH$_3)_3$, d, $J_{H\text{-}H}$ = 5.4 Hz), 4.33 (1H, OC*H*$_2$C(CH$_3)_3$, d, $J_{H\text{-}H}$ = 5.4 Hz), 4.19 (1H, OC*H*$_2$C(CH$_3)_3$, d, $J_{H\text{-}H}$ = 5.4 Hz), 2.98 (3H, OBzA, s), 1.03 (9H, OCH$_2$C(C*H*$_3)_3$, s), 0.99 (9H, OCH$_2$C(C*H*$_3)_3$, s). Anal. Calcd for $C_{107}H_{136}O_{28}Ti_4$ (%): C, 62.33; H, 6.65. Found: C, 62.33; H, 6.50.

2.5. *[[(OPr^i)$_3$Ti(μ-OPr^i)Ti(OPr^i)$_2$]$_2$(μ-(μ$_c$,μ-OBzA))$_2$]$_2$ (4)*

Used [Ti(OPr^i)$_4$] (2.00 g, 7.04 mM), H_2-OBzA (0.958 g, 3.52 mM), and toluene (~7 mL). Yield 51.0% (1.29 g). FTIR (KBr, cm^{-1}) 2953(s), 2904(m), 2866(m), 2844(m), 1592(s), 1521(s), 1500(w), 1490(w), 1460(w), 1419(m), 1393(w), 1374(m), 1259(m), 1216(m), 1171 (w), 1122(s), 1089(s), 1023(m), 979(w), 930(w), 869(w), 843(w), 814(w), 780(w), 750(w), 733(w), 696(m), 665(w), 630(w), 604(w), 539(w), 477(w). ^{1}H NMR (500.1 MHz, tol-d_8) d 8.16 (1H, OBzA d, $J_{H\text{-}H}$ = 3.9 Hz), 7.09–7.03 (4.2H, OBzA and free tol, mult), 6.96 (2H, OBzA, t, $J_{H\text{-}H}$ = 7.5 Hz), 6.88 (1H, OBzA, t, $J_{H\text{-}H}$ = 7.6 Hz), 6.12 (1H, OBzA, d, $J_{H\text{-}H}$ = 4.5 Hz), 5.91 (1H, OBzA, s), 5.08 (1H, OC*H*$(CH_3)_2$, sept, $J_{H\text{-}H}$ = 6.1 Hz), 4.81 (1H, OC*H* $(CH_3)_2$, sept, $J_{H\text{-}H}$ = 6.1 Hz), 4.51 (2H, OC*H*$(CH_3)_2$, sept, $J_{H\text{-}H}$ = 6.1 Hz), 2.98 (3H, OBzA,

s), 1.38, (3H, OCH(CH_3)$_2$, d, $J_{H\text{-}H}$ = 6.1 Hz), 1.34 (3H, OCH(CH_3)$_2$, d, $J_{H\text{-}H}$ = 6.1 Hz), 1.27 (27H, OCH(CH_3)$_2$, d, $J_{H\text{-}H}$ = 6.1 Hz), 1.19 (3H, OCH(CH_3)$_2$, d, $J_{H\text{-}H}$ = 6.1 Hz). Anal. Calcd for $C_{66}H_{104}O_{22}Ti_4$ (MW = 1440.99) 55.01%, C; 7.27%, H. Anal. Calcd for $C_{80}H_{120}O_{22}Ti_4$ (%): C, 59.12; H, 7.44. Found: C, 58.63; H, 7.77.

2.6. *[(ONep)$_3$Zr(μ-ONep)$_2$Zr(ONep)$_2$]$_2$(μ-(c,μ-OBzA))$_2$ (5) •tol*

Used [Zr(ONep)$_4$] (0.500 g, 1.05 mM), H_2-OBzA (0.143 g, 0.525 mM), and toluene (~5 mL). The reaction was then dried *in vacuo*, redissolved in THF, and crystals grown by cooling to −45 °C. Yield 80.0% (0.409 g). FTIR (KBr, cm^{-1}) 2951(s), 2904(m), 2866(s), 2760(m), 1617(s), 1604(s), 1559(s), 1519(s), 1482(m), 1461(m), 1446(m), 1410(s), 1381(m), 1363(m), 1262(s), 1220(m), 1167(s), 1124(s), 1026(m), 1001(s), 979(w), 925(w), 837(w), 780(w), 762 (w), 728(w), 712(w), 654(m), 632(m), 587(w), 464(m). ^{1}H NMR (500.1 MHz, THF-d$_8$) δ 7.58–7.52 (2H, OBzA, mult), 7.28 (1H, OBzA, mult), 7.19 (1H, OBzA, mult), 6.90 (1H, OBzA, mult), 6.37 (1H, OBzA, d), 6.15 (1H, OBzA, mult) 3.84 (8H, OCH_2C(CH$_3$)$_3$, s), 3.59 (8H, OCH_2C(CH$_3$)$_3$, s), 0.92, 0.87, 1.18 (36H, OCH$_2$C(CH_3)$_3$, s and mult). Anal. Calcd for $C_{90}H_{152}O_{22}Zr_4$ (%): C, 55.40; H, 7.85. Found: C, 55.22; H, 8.12.

2.7. *[(py)(OBu^t)$_3$Zr]$_2$(μ-(c,c-OBzA)) (6)*

Used [Zr(OBu^t)$_4$] (0.423 g, 1.10 mM), H_2-OBzA (0.150 g, 0.550 mM), and pyridine (~10 mL). Yield 35.6% (0.224 g). FTIR (KBr, cm^{-1}) 2967(s), 2939(m), 2924(w), 2863(w), 1612 (s), 1594(s), 1579(s), 1561(s), 1520(s), 1440(m), 1402(s), 1374(s), 1358(s), 1254(s), 1219 (s), 1204(s), 1168(s), 1123(m), 1092(m), 1034(s), 1005(s), 980(m), 926(m), 854(w), 839 (w), 808(w), 728(m), 762(w), 726(m), 658(w), 627(w), 602(m), 573(w), 539(m), 484(w), 434(w). ^{1}H NMR (500.1 MHz, tol-d$_8$, partial: aryl peaks of OBzA not distinguishable) d 8.71 (4H, py, bs), 7.55 (2H, py, bs), 7.19 (4H, py, bs), 3.63 (3H, OCH_3, s), 1.40 (54H, OC (CH_3)$_3$, s). Anal Calcd for $C_{49}H_{74}N_2O_{11}Zr_2$ (%): C, 56.07; H, 7.11; N, 2.67. Found: C, 60.13; H, 6.18; N, 1.54.

2.8. *[(OBu^t)$_2$Hf(μ-OBu^t)]$_2$(μ-(c,η^1-OBzA)) (7)*

Used [Hf(OBu^t)$_4$] (0.520 g, 1.10 mM), H_2-OBzA (0.150 g, 0.552 mM), and toluene (~10 mL). The reaction was then dried *in vacuo*, redissolved in THF, and crystals grown by cooling to −45 °C. Yield 23.9% (0.141 g). FTIR (KBr, cm^{-1}) 3068(w), 2973(s), 2925(m), 2898 (m), 2866(w), 1593(s), 1522(s), 1499(m), 1441(m), 1419(s), 1372(s), 1339(w), 1269(s), 1253(s), 1218(s), 1193(s), 1169(s), 1121(s), 1089(m), 998(s), 929(m), 868(m), 842(w), 793 (m), 779(m), 768(w), 731(m), 712(w), 666(m), 631(m), 604(m), 588(m), 486(m), 467(m). ^{1}H NMR (500.1 MHz, THF-d$_8$) d 8.53 (1H, OBzA s(br)), 7.65 (1H, OBzA, s(br)), 7.24 (1H, OBzA, s(br)), 6.91 (1H, OBzA, s(br)), 6.74 (1H, OBzA, s(br)), 5.84 (1H, OBzA, s (br)), 3.19 (3H, OBzA, s(br)), 1.77 (42H, OC(CH_3)$_3$, s). Anal. Calcd for $C_{39}H_{64}Hf_2O_{11}$ (%): C, 43.95; H, 6.05. Found: C, 43.69; H, 5.88.

2.9. *General X-ray crystal structure information*

Single crystals were mounted onto a loop from a pool of Fluorolube™ and immediately placed in a cold N_2 vapor stream on a Bruker AXS diffractometer employing an incident-beam

graphite monochromator, Mo Kα radiation ($L = 0.71070$ Å), and a SMART APEX CCD detector. Lattice determination and data collection were carried out using SMART Version 5.054 software. Data reduction was performed using SAINTPLUS Version 6.01 software and corrected for absorption using the SADABS program within the SAINT software package. Structures were solved by direct methods or by using the PATTERSON method that yielded the heavy atoms, along with a number of lighter atoms. Subsequent Fourier syntheses yielded the remaining light-atom positions. Hydrogens were fixed in positions of ideal geometry and refined using SHELX software. The final refinement of each compound included anisotropic thermal parameters for all non-hydrogen atoms. All final CIF files were checked using the CheckCIF program (http://www.iucr.org/). Additional information concerning the data collection and final structural solutions can be found in the supplemental information or by accessing CIF files through the Cambridge Crystallographic Data Base. Table 1 lists the unit cell parameters for the structurally characterized **1–7**.

Specific issues related to the structure solution of **1–7** are discussed below. For **2**, **3**, **4**, **5**, **6**, and **7** volumes of 333.0 (THF), 491.4 (toluene), 495.6 (toluene) 448.9 (toluene), 644 (pyridine), and 2491.2 (four THF or toluene) Å^3, respectively, were modeled by the squeeze program. The disorder observed for several of the carbons in **1**, **2**, **3**, and **5** was modeled using EADP and DFIX. Disorder in the ONep ligands in **5** was modeled using PART instructions. In addition for **5**, C46, C47, C50, and the H atoms are all half-weighted to account for the mirror plane that splits the toluene molecule. The data collected for **5a** suffer from an extremely high R_{int} and **5b** was found to possess significant disorder in the *t*-Bu groups of the ONep ligands. These phenomena significantly limit the acceptability of the final structures. While the central core is unequivocally identified, the final structure is not of high enough quality to allow for discussion of the metrical data. Therefore, we have presented the parameters for the unit cell in table 1 for rapid identification of the complex, but have not included the information in the final crystallographic data-set.

3. Results and discussion

There are no structural reports of any transition metal modified by the OBzA framework (two methylene-linked aromatic rings with one possessing an oxygen and one a carboxylate moiety) [10]. However, there are some reports concerning the structure of chloro- [13, 14] or bromo- [15] substituted 2-(2′-hydroxybenzoyl)-benzoic acids (note: these are the acids only, no transition metal are present). Therefore, the initial research effort reported here focused on determining the coordination behavior of this unusual multifunctional, 2-benzophenone derivative (H_2-OBzA) in the presence of [$M(OR)_4$].

3.1. *Synthesis*

Upon addition of the H_2-OBzA ligand, the clear colorless solution of the various [$M(OR)_4$] in toluene (equation (1)) turned yellow. Removal of the solvent after stirring for 12 h led to a yellow powder for each reaction. The loss of the –OH stretches of the OBzA ligand in the FTIR spectrum proved to be an adequate means to determine the endpoint for each reaction. In addition, a shift of the carboxylate stretches from 1691 to ~1591 cm^{-1}, carbonyl stretch from 1625 to ~1550 cm^{-1}, and the keto stretches from 1593 to ~1522 cm^{-1} for **1–3**

Table 1. Data collection parameters for **1–7**.

Compound	**1** •2tol	**2** •THF	**3**
Chem. form.	$C_{98}H_{111}O_{28}Ti_4$	$C_{96}H_{120}O_{29}Ti_4$	$C_{100}H_{119}O_{28}Ti_4$
Form. weight	1928.35	1929.52	1960.43
Temp. (K)	100	100	100
Space group	*P-1*	*P-1*	*P-1*
a (Å)	11.7645 (5)	18.0938 (6)	11.2384 (8)
b (Å)	19.6520 (9)	18.8067 (7)	17.2792 (13)
c (Å)	22.4007 (10)	19.3182 (7)	30.993 (2)
α (°)	112.298 (2)	67.414 (2)	89.999 (5)
b (°)	90.361 (3)	63.446 (2)	89.953 (5)
γ (°)	98.310 (3)	70.585 (2)	83.518 (5)
V (Å^3)	4730.8 (4)	5325.5 (3)	5980.1 (7)
Z	2	2	2
D_{Calcd} (Mg m^{-3})	1.354	1.203	1.089
μ (Mo Kα) (mm^{-1})	0.404	0.359	0.320
[a]*R1* (%) (all)	6.66 (10.60)	8.22 (13.98)	8.42 (18.46)
[b]*wR2* (%) (all)	17.48 (21.07)	22.43 (24.40)	21.19 (24.23)

Compound	**4**	**5** •tol	**5a**
Chem. form.	$C_{66}H_{104}O_{22}Ti_4$	$C_{97}H_{160}O_{22}Zr_4$	$C_{90}H_{153}O_{22}Zr_4$
Form. weight	1441.09	2043.12	1951.00
Temp. (K)	100	100	100
Space group	*P21/n*	*C2/c*	*C2/c*
a (Å)	11.6089 (3)	24.1423 (18)	28.9560 (8)
b (Å)	21.2296 (7)	18.0020 (11)	19.1622 (6)
c (Å)	16.7934 (5)	28.058 (2)	18.7024 (5)
α (deg)			
b (deg)	109.318 (2)	109.316	102.326 (2)
γ (deg)			
V (Å^3)	3905.7 (12)	11507.8 (14)	10,138
Z	2	4	4
D_{Calcd} (Mg/m^3)	1.225	1.179	1.278
μ (Mo Kα) (mm^{-1})	0.460	0.411	0.459
[a]*R1* (%) (all)	5.76 (9.17)	7.09 (16.02)	8.70 (33.56)
[b]*wR2* (%) (all)	16.54 (17.99)	16.20 (19.89)	18.43 (28.04)

Compound	**5b**	**6**	**7**
Chem. form.	$C_{82}H_{126}O_{23}Zr_4$	$C_{49}H_{74}N_2O_{11}Zr_2$	$C_{39}H_{64}Hf_2O_{11}$
Form. weight	1844.70	1049.54	1065.88
Temp. (K)	100	100	100
Space group	*C2/c*	*P-1*	*P21/n*
a (Å)	28.5222 (2)	9.8674 (5)	25.1937 (16)
b (Å)	11.7372 (7)	15.8393 (9)	10.5321 (6)
c (Å)	27.0049 (18)	20.3481 (11)	40.492 (2)
α (deg)		85.577 (4)	
b (deg)	100.007 (6)	81.069 (4)	95.852 (5)
γ (deg)		83.010(4)	
V (Å^3)	8902.9 (10)	3112.8 (3)	10688.3 (11)
Z	4	2	8
D_{Calcd} (Mg/m^3)	1.376	1.120	1.325
μ (Mo Kα) (mm^{-1})	0.523	0.382	3.926
[a]*R1* (%) (all)	7.00 (16.60)	8.06 (10.74)	4.04 (6.43)
[b]*wR2* (%) (all)	15.97 (24.81)	21.69 (24.38)	13.03 (14.20)

[a]$R1 = \Sigma||F_o|-|F_c||/\Sigma|F_o| \times 100$.
[b]$wR2 = [\Sigma w\,(F_o^2-F_c^2)^2/\Sigma\,(w|F_o|^2)^2]^{1/2} \times 100$.

indicated the reaction had proceeded to completion [16–18]. For **4**, the shift is also similar for carboxylate and keto-carbonyl (1592 and 1521 cm^{-1}, respectively); however, substantially more bends and stretches are noted that were associated with $Ti(OPr^i)_4$. Similar carboxylate and keto-carbonyl shifts were observed for the larger congeners with stretches at 1579 and 1520 cm^{-1} for **5**, 1594 and 1520 cm^{-1} for **6**, and 1593 and 1522 cm^{-1} for **7**. These shifts are consistent with an asymmetric interaction between these functional groups and the various metal centers for each compound [19–28]. In addition, the appropriate stretches and bends for the parent ORs were present with a substantial change in the fingerprint region. Therefore, based on the isolation of yellow powders for each reaction coupled with the FTIR data, the bulk powders appeared to have reacted with the functional groups of the OBzA ligands.

3.2. *X-ray structures*

Due to the limited structural information that could be ascertained from the FTIR spectrum, single-crystal X-ray diffraction studies were undertaken. These are discussed below based on the metals: (1) Ti, (2) Zr, and (3) Hf. Due to the complexity of the OBzA ligand-binding modes, a brief explanation of the abbreviations used is warranted. The first symbol (outside of the parenthesis) refers to the overall functionality of the OBzA ligand. The first symbol in the parentheses refers to the hydroxyl/carbonyl coordination and the second to the carboxylate bonding. Therefore, for μ-(c, μ)OBzA arrangement shown in figure 1(e), the OBzA ligand bridges between metals with a chelation of hydroxyl and carbonyl oxygens to one metal with the carboxylate acting as a bridge between two other metals.

3.2.1. Titanium. The 1 : 1 reaction between $[Ti(OR)_4]$ (OR = OPr^i, OBu^t, and ONep) and the H_2-OBzA led to the isolation of crystals for each reaction. Similar dinuclear structures were solved for **1–3** and are shown in figures 2–4, respectively. For these compounds, the OBzA ligands bridge the two distorted octahedral (*OC*-6) bound Ti metal centers in a C_2 arrangement. Each metal coordinates two oxygens from a chelating carboxylate of one of the OBzA ligands and the hydroxide and carbonyl oxygen (in a chelating mode) from the other OBzA ligand. The final two coordination sites on Ti are filled by the remaining parent alkoxide ligands. The μ-(c,c)OBzA notation [see figure 1(d)] was used to represent the binding mode of the OBzA molecule between Ti metal centers.

For the larger OR (ONep or OBu^t) ligands, an increase in the metal stoichiometry did not lead to additional coordination around the H_2-OBzA ligand but instead again led to isolation of **2** and **3**. However, the 2 : 1 $Ti(OPr^i)_4$: H_2-OBzA reaction mixture was found to generate the tetranuclear **4** (see figure 5). For **4**, each of the four Ti centers was solved in distorted *OC*-6 geometry using O atoms from the OBzA and OPr^i ligands. The four Ti ions are roughly linearly aligned and bind to at least one oxygen from each of the OBzA ligands. For Ti(1), three terminal OPr^i, one μ-OPr^i, and one carboxylate oxygen of OBzA (1), and a μ-O from the hydroxide of OBzA(2) ligand are used to fill the *OC*-6 geometry. The bridging oxygens bind to Ti(2) which finishes its *OC*-6 coordination using two terminal OPr^i, the other OBzA(1) carboxylate oxygen, and the carbonyl from OBzA(2). The remainder of the molecule is a reflection of the first half, yielding C_2 symmetry. The μ-(μ_c,μ)OBzA notation [figure 1(f)] conveniently represents the various OBzA interactions described above.

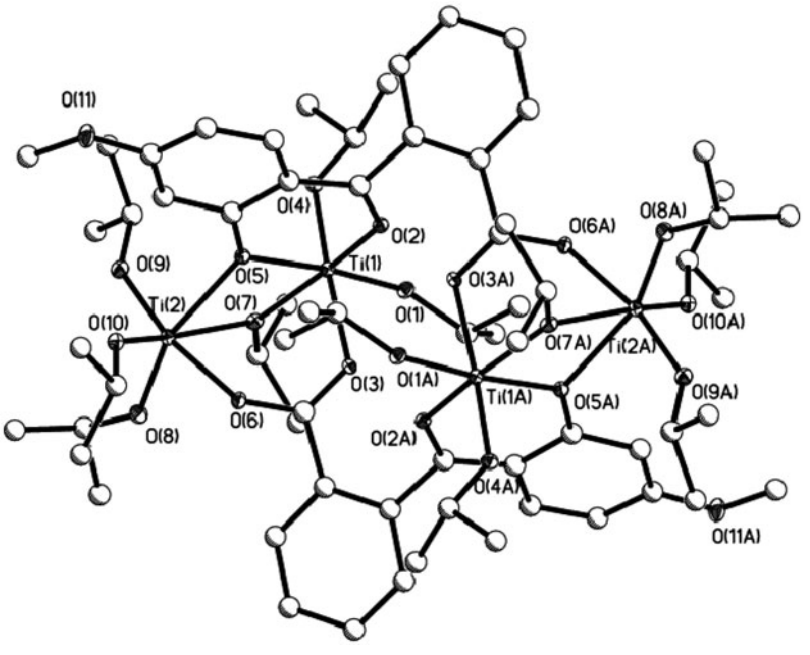

Figure 5. Structure plot of **4**. Thermal ellipsoids of heavy atoms are drawn at the 50% level and carbons are shown as stick and ball for clarity.

Table 2. Select average metrical data for **1–7**.

Av. Distances (Å)	**1**	**2**	**3**	**4**	**5**	**6**	**7**
M–OR	1.78	1.77	1.76	1.77	1.92	1.94	1.92
$M–O_{OBzA\ (OH)}$	1.93	1.92	1.92	1.92	2.06	2.13	2.04
$M–O_{OBzA\ (C=O)}$	2.11	2.12	2.09	2.09	2.16	2.30	2.32
$M–O_{OBzA\ (O2C)}$	2.16	2.17	2.16	2.16	2.22	2.31	2.05
$M–N_{py}$	–	–	–	–	–	2.45	–
Av. Angles (Å)	**1**	**2**	**3**	**4**	**5**	**6**	**7**
OR–M–OR	102.3	103.7	102.2	102.2	101.0	102.5	101.6
$O_{OH}–M–O_{C=O}$	82.0	82.0	82.3	82.3	77.2	74.8	78.5
$O_{(O2C)}–M–O_{(O2C)}$	60.7	60.5	60.7	60.7	–	56.8	–
O–C–O	118.5	118.4	118.4	118.5	123.8	119.8	123.2
$C–C_{C=O}–C$	121.0	121.4	119.2	119.4	119.9	120.3	116.9

Note: – not present.

The metrical data for **1–4** were evaluated collectively and compared to literature $[Ti(OR)_4]$ compounds as well as the literature model $[(ONep)_2Ti(\mu\text{-}ONep)]_2(\mu\text{-}OBzP)$ [8]. Table 2 lists the average metrical data for select bond distances and angles for **1–4**. The Ti–OR distances (av. 1.77 Å) and angles are consistent with existing $[Ti(OR)_4]$ compounds [10] and with the OBzP compound (1.79 Å). The Ti–O distances recorded for the central core of OBzA compared to the OBzP complex are similar [M–O of OBzA *versus* OBzP : hydroxyl (1.92 Å *versus* 1.87 Å) and carbonyl (2.10 Å *versus* 2.19 Å)] where variations in

distances are attributed to the carboxylate (M–O = 2.16 Å). The change to OBzA ligand also led to variations in the angles noted for the central constructs, such as the O–M–O angle reported for the hydroxyl-carbonyl oxygens, which were significantly more acute for the OBzA (82.2°) compounds *versus* the OBzP (87.1°) derivative. The C–C(=O)–C angle shows the strain for the OBzA compounds 120.2° *versus* 123.6° for OBzP. The torsion angle of the linked phenyl of the OBzA ranges from 70.9° to 86.8° for **1–3**; however, for the sterically encumbered OBzA rings of **4** a much smaller 57.7° torsion angle was recorded.

3.2.2. Zirconium. Switching to the larger Zr center, a more complex coordination behavior of the OBzA ligand was noted in the structures isolated. Independent of the stoichiometry, each compound isolated proved to be the 2 : 1 (M : OBzA) product. Surprisingly, for the Zr-OBzA-ONep family several different isomers were solved. The initial species isolated from toluene was the tetranuclear complex **5** (figure 6) that possesses a C_2 center of symmetry, where each Zr was found to be in an *OC*-6 geometry. In one half of the molecule, a dimeric "$(ONep)_3Zr(1)(\mu\text{-}ONep)_2Zr(2)(ONep)$" moiety was solved with the final coordination sites of Zr(1) filled by carboxylate oxygen of OBzA(1). For the other Zr(2) of the same dimer, the other carboxylate oxygen of OBzA(1) and the hydroxide and keto-carbonyl of OBzA(2) complete its coordination geometry. The other OBzA(2) ligand bridges in a similar manner to the other "$(ONep)_3Zr(\mu\text{-}ONep)_2Zr(ONep)$" moiety. This results in the two "$(ONep)_3Zr(1)(\mu\text{-}ONep)_2Zr(2)(ONep)$" bridged by carboxylate oxygens of one OBzA ligand and the hydroxyl/carbonyl on the other [figure 7(a)]. The final coordination was assigned as a μ-(c,μ)OBzA coordination [figure 1(e)].

Attempts to generate improved quality crystals of **5** by recrystallization of the dried powder in THF under an atmosphere of argon led to the isolation of **5a** and **5b** (isolated from different attempts). Compound **5a** [figure 7(b)] is an identical arrangement as noted for **5**. However, the torsion angle of the two OBzA ligands is more acute at 108.0° in

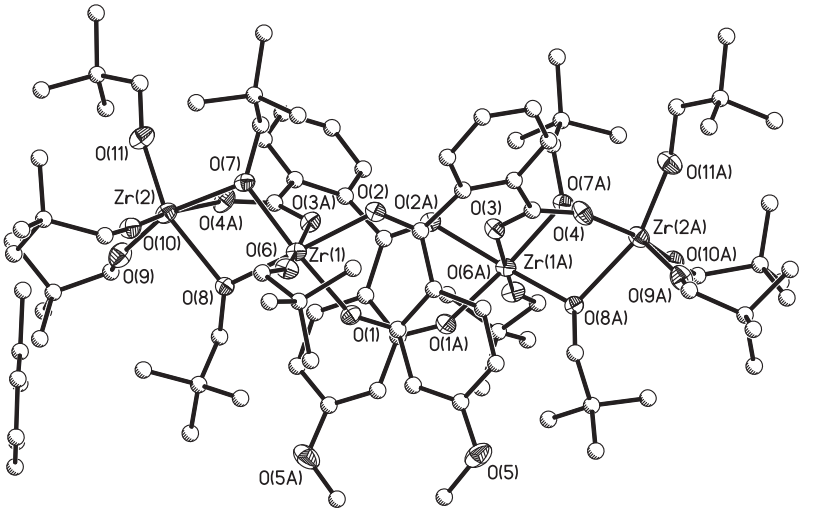

Figure 6. Structure plot of **5** •tol. Thermal ellipsoids of heavy atoms are drawn at the 50% level and carbons are shown as stick and ball for clarity.

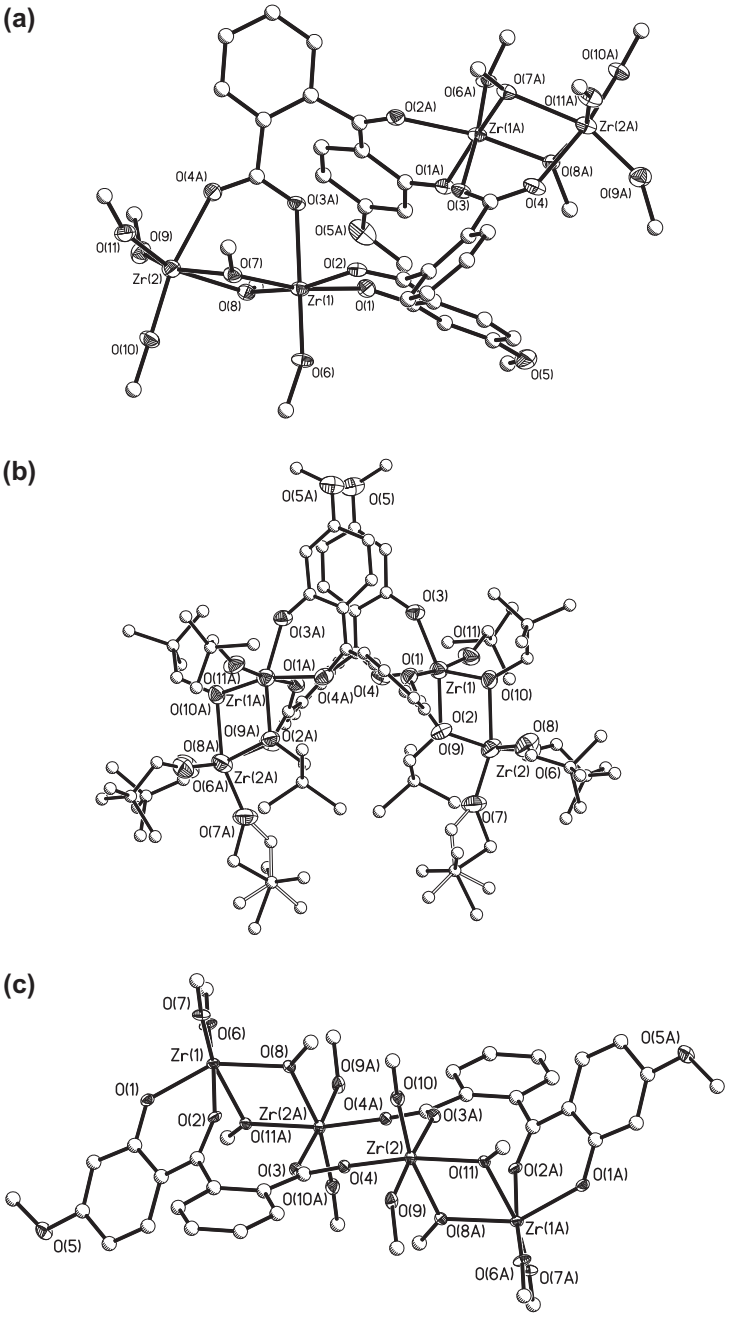

Figure 7. Structure plot of central core of (a) **5**, (b) **5a**, and (c) **5b**. Thermal ellipsoids of heavy atoms are drawn at the 50% level. Majority of carbons have been removed for clarity.

comparison to the 126.4° observed for **5** [figure 7(a)]. This variation may be due to increased packing strain based on lack of solvent in **5** compared to the two toluene molecules present in **5**. This results in a slightly different unit cell (table 1). Another attempt led

to the isolation of **5b** [figure 7(c)]. For this complex, each Zr was again in an *OC*-6 geometry along with the previously observed "$(ONep)_3Zr(1)(\mu\text{-}ONep)_2Zr(ONep)$" moiety; however, for **5b** the bridging behavior of the OBzA ligand is different from **5** or **5a**. For **5b**, the carboxylate oxygens of the two OBzA ligands span the two "$(ONep)_3Zr(1)(\mu\text{-}ONep)_2Zr(ONep)$" moieties. The hydroxyl and carbonyl oxygens bind to Zr(1) of the first "$(ONep)_3Zr(1)(\mu\text{-}ONep)_2Zr(ONep)$" fragment with the carboxylate binding to Zr(2a) and bridging to Zr(2) of the other moiety. The other OBzA ligand binds in a symmetrical manner. This also places the OBzA ligand as μ-(c,μ)OBzA [figure 1(e)] but the carboxylate moieties hold the two Zr dimers together. Crystals isolated from the Lewis basic solvent pyridine led to **6**. Again, two Zr ions are present but there is only one OBzA ligand. The solved structure of **6** is shown in figure 8. In this structure, the OBzA ligand acts as a bridge with the hydroxide and ketyl-carbonyl oxygens chelating to one Zr and a chelating carboxylate on the other Zr (or μ-(c,c)OBzA [figure 1(d)]. The *OC*-6 geometry of each Zr center was filled by three OBu^t and a coordinated py. These compounds demonstrate the complicated arrangements available to the OBzA ligand.

A comparison of the metrical data for **5** and **6** (table 2) was undertaken against the OBzP model compounds, $[(ONep)_2Zr(\mu\text{-}ONep)]_2(\mu\text{-}OBzP)$, $[(ONep)_2Zr(\mu\text{-}OBzP)]_2$ and $[(ONep)_2(OBzP)Zr(\mu\text{-}ONep)Zr(py)(\mu_3O)]_2$, due to some similarity in construction [8]. The OBzP derivatives have Zr–OR distances (av. 1.94 Å) and angles that are consistent with **5** and **6**. The Zr–O distances recorded for the central core of the OBzA compared to the OBzP complex are similar [M–O of OBzA *versus* OBzP : hydroxyl (2.09 Å *versus* 2.03 Å) and carbonyl (2.23 Å *versus* 2.26 Å)], where variations in distances are attributed to the "carboxylate moiety" (M–O = 2.26 Å). The O–M–O angle reported for the hydroxyl-carbonyl oxygens, which were similar for the OBzA (76.0°) compounds *versus* the OBzP (76.8°) derivatives. The C–C(=O)–C angle shows the similarity of the strain for the OBzA compounds (120.1°) *versus* 119.1° for the OBzP. The torsion angle of the rings for **5** and **6** range from 50.9° to 70.8°.

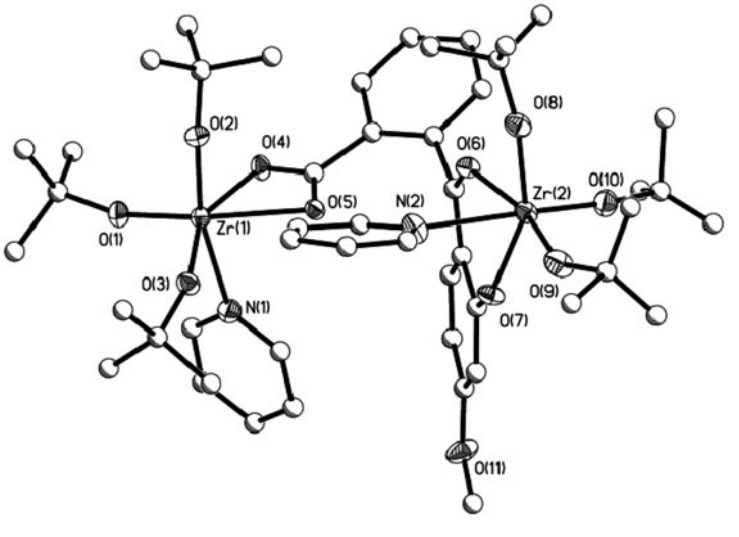

Figure 8. Structure plot of **6** •tol. Thermal ellipsoids of heavy atoms are drawn at the 50% level and carbons are shown as stick and ball for clarity.

3.2.3. Hafnium. The change in the behavior of the OBzA and subsequent reduction in nuclearity observed for Zr was thought to be due to the combination of the larger OBu^t, the introduction of the Lewis basic solvent, and the larger cation. Therefore, it was expected that similar compounds would be observed for the Hf derivatives (six-coordinate Zr (0.86 Å) is similar in size to the *OC*-6 Hf (0.85 Å)) [29]. However, additional influences from Hf led to new structure types. For **7** (figure 9), a dinuclear compound was solved forming a "$(OBu^t)_4Hf_2(\mu\text{-}OBu^t)$" core that was bridged by a single unusual binding mode of the OBzA ligand while the hydroxide and carbonyl chelate to the same metal and the carbonyl oxygen bridges to the other Hf as previously observed. But due to this arrangement, there is not enough room to have the carboxylate chelate, thus only one oxygen binds to the second Hf. This results in an unusual η^1-binding mode by the carboxylate, thus forming a μ-(c, η^1)OBzA arrangement as shown in figure 1(c).

The angles and distances noted for **7** were in line with the other OBzA derivatives, when the cation size was accounted for. The angles around Hf centers were consistent with a distorted *OC*-6. A good model system to compare to **7** is the OBzP derivative $(OBu^t)_2Hf_2(\mu\text{-}OBu^t)_2(\mu\text{-}OBzP)$ [8]. The terminal Hf–OR distances and angles (table 2) were in agreement with this compound as well as with the literature values that ranged from 1.89 to 2.22 Å [10]. The bridging Hf–(μ-OR) distance (av. 2.17 Å) and Hf–(μ-OR)–Hf angle (av. 98.4°) observed for **7** were also consistent with the OBzP species (av. 2.17 Å and 97.8°, respectively) [8] and within the range reported for similar literature compound (2.09–2.23 Å and 93.8° and 115.1°). The Hf–O (carbonyl) distance of 2.32 Å of **7** was similar to the 2.40 Å noted for the OBzP derivative but the (hydroxyl)O–Hf–O (carbonyl) angle was slightly compressed for the OBzP (76.5°) in comparison to **7** [8]. The Hf–(μ-OR)–Hf angles were found to fall at the short end of the literature reports and this phenomenon is most likely due to the OBzA-imposed constraints.

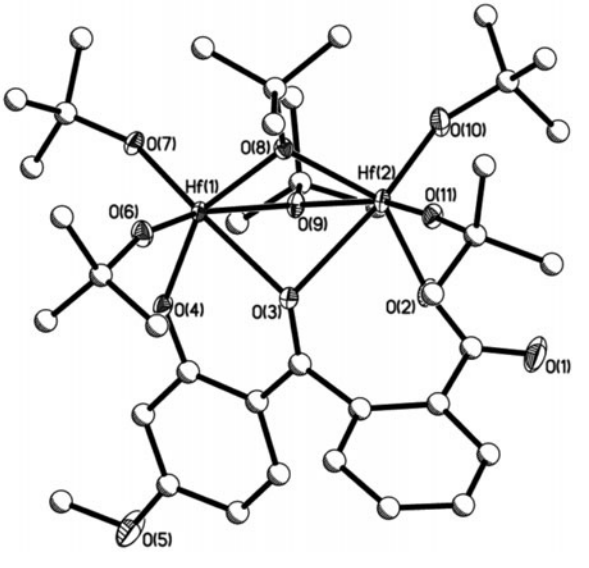

Figure 9. Structure plot of **7**. Thermal ellipsoids of heavy atoms are drawn at the 50% level and carbons are shown as stick and ball for clarity. Two *iso*-structural molecules were solved in the unit cell but only a single molecule is shown.

3.3. *Solution NMR*

Solution NMR spectra were collected for **1–7** to assist in determining if their structures were retained in solution and in determining the purity of the bulk powder. The crystalline materials were dissolved in the appropriate deuterated solvent and then vacuum-sealed in an NMR tube. The low solubility of **1–7** led to ^{13}C NMR spectra that did not add much detail concerning the structural behavior of the various compounds studied and these data are not presented. However, the ^{1}H NMR spectral data were useful in tentatively establishing the solution structural behavior for these compounds.

For **1–3**, if the solid-state structures are retained upon dissolution, the C_2 center of symmetry suggests that seven phenoxide resonances, a single OMe singlet, and two sets of OR resonances should be observed. The resulting ^{1}H NMR spectra of **1–3** were consistent with the expected resonances. For **1**, in addition to the six phenyl resonances (one overlap of resonances was noted based on integration) and the singlet for the OMe group of the OBzA ligand, there are two septuplets and four doublets noted for the OPr^{i} ligands. This is consistent with two inequivalent OPr^{i} where the methyl groups are diastereotopic due to the restricted rotation caused by the rigid OBzA ligand. For **2**, five of the seven expected peaks associated with the OBzA aryl protons were noted due to obfuscation by the tol-d_8 resonances. In addition, there are three singlets clearly present for the OMe of the OBzA and two approximately equal OBu^{t} methyl group resonances. This again indicates the structure is retained with the OBu^{t} ligands being inequivalent due to hindered rotation. For **3**, a similar spectrum was observed with six phenyl resonances. The ONep ligands are diastereotopic, which results in two types of methyl resonances and four methylene resonances. The Bu^{t} groups of ONep are far enough removed from the steric congestion of the OBzA ligands, that they are free to rotate thus equating the methyl groups; however, the methylene resonances are "locked in" and four diastereotopic doublets were observed. Based on these data, retention of the structures of **1–3** in solution is expected.

Compound **4** also possess a C_2 center of symmetry, which should lead to seven aryl, one OMe, and six sets of OPr^{i} resonances. The experimental spectrum of **4** revealed a similar spectrum noted for **1**, with one additional set of large OPr^{i} resonances (septuplet and doublet). The ratio of the two smaller to larger OPr^{i} methine resonances was in 1 : 1 : 2 pattern. It is hard to account for this ratio with the existing solid-state structure. One possible explanation for this particular ratio is that one of the μ-OPr^{i} moieties forms a bond upon dissolution and becomes a bridging OPr^{i}. If this occurs, then there would be six terminal, three bridging, and three internally bound terminal OPr^{i} (or 1 : 1 : 2 ratio), leaving the rest of the structure similar to that of **1**. This would result in a seven-coordinate Ti, which are well established in the solid state [10] and could be easily obtained in solution. Further, the symmetry of **4** would be destroyed by this dynamic behavior resulting in a doubling of resonances (14 aryl, 2 OMe, 12 methyl resonances); however, these resonances would be expected to be very similar. The methyl resonances were found in a 1 : 1 : 9 : 1 ratio, which is consistent with the expected overall integration for these peaks. Due to the similarity of the majority of the methyl groups either by symmetry or dynamic behavior, their respective peak overlap explains the larger peak. For the more unique and locked out methyl groups (i.e. the small resonances), a slight chemical shift is noted. Based on this, the general structural arrangement appears to be retained in solution for **4**.

The introduction of the larger Zr cation produced **5**, which is more complicated than the Ti derivatives, but again a similar set of resonances should be noted: seven for the aryl protons, one for the OMe group, and six sets of ONep resonances. The observed spectrum

consisted of the expected number of OBzA resonances, but only two methylene ONep resonances were observed with a number of single methyl resonances that were grouped together. Due to the difficulty in isolating each one they were reported as a multiplet with the cumulative integration.

The structure of **6** was expected to give the standard seven phenyl resonances and two sets of OBu^t due to the asymmetric binding mode of the OBzA ligand. Only a single OBu^t resonance was observed, which is most likely due to coincidental overlap due to the similar environments of the two metal centers. Since the elemental analysis of the bulk powder proved inconclusive, the results from these data indicate that the bulk powder is consistent with the single-crystal structure (*vide supra*).

While **7** was successfully crystallized from THF, the crystals proved to have low solubility in THF-d_8 and no solubility in tol-d_8. The spectrum isolated in THF-d_8 revealed a majority of the expected OBzA resonances (overlap with residual toluene made detection of all the resonances difficult) along with one singlet for the μ-OBu^t and another for the terminal OBu^t ligands. The breadth of this resonance was thought to be indicative of dynamic exchange of the two sets (μ- and terminal) of OBu^t ligands. From these data, it appears that the compounds are relatively pure with the general connectivity of **1–7** retained in solution.

3.4. *Elemental analysis*

Elemental analyses were conducted to assist in determining the purity of dried crystalline powders of **1–7**. Compositional calculations were based on the metal-OBzA moiety, which would *not* include the lattice solvent. Typically, $[M(OR)_4]$ do not yield acceptable elemental analyses due to properties that make them of interest for materials production (i.e. high volatility, rapid hydrolysis and condensation, low decomposition temperatures, etc.). Obtaining acceptable analyses are further complicated when solvents are bound due to their premature loss or inclusion of spurious solvent molecules. Therefore, it is not surprising that the bulk powders of **1–4** were not in agreement with the single-crystal structures; however, when the solvent lattice atoms are removed/added [for **1** (−2 lattice tol) or **2** (−1 lattice THF)) or added (for **3** (+1 tol) and **4** (+2 tol), **5** (−tol lattice)], percentages are obtained that are in agreement with the values calculated from their respective single-crystal structure. For both **3** and **4**, the addition of solvent is consistent with the "squeeze"-removed solvents used for the final model. Based on the elemental analysis data, these bulk powders can be considered to be consistent with the single-crystal structures. For **6**, an acceptable analysis could not be achieved; however, the loss of a pyridine molecule and addition of a toluene molecule brings the values close to an acceptable value, but these are still outside of the allotted range. Therefore, the identification of the bulk powder of **6** could not be confirmed by elemental analysis; however, NMR data (*vide infra*) did indicate the bulk powder was consistent with **6**. The elemental analysis of the bulk powder of **7** was consistent with the calculated values from the single-crystal structure.

4. Conclusion

For the first time, coordination behavior of H_2-OBzA with a transition metal was determined. Using Group 4 $[M(OR)_4]$, the OBzA derivatives were identified as dinuclear (**1**, **2**,

3, **6**, and **7**) and tetranuclear (**4** and **5**) species. The OBzA ligand utilized every functional site available and acted as a bridging ligand for the various $[M(OR)_4]$ studied. With the disparate functional groups proximally located, some unusual bonding modes were observed [figure 1(c): μ-(c, η^1)OBzA was observed for **7**; figure 1(d): μ-(c, c)OBzA was solved for **1**, **2**, **3**, and **6**; figure 1(e): μ-(c, μ)OBzA was noted for **5**, and figure 1(f): μ-(μ_c, μ)OBzA was the bonding mode for **4**]. The carbonyl/hydroxide (OH/C=O) combination resulted in chelation for all the compounds identified in this report; however, for **4**, the hydroxide also bridged. The carboxylate ranged from simple chelation (**1–3**, **6**) to bridging (**4** and **5**) but was never solved in both a chelating and bridging manner. For **7**, an unusual η^1 interaction was observed for the carboxylate. Complex bonding modes noted for **1–7** indicate a great deal of flexibility in the coordination of the OBzA ligand and mixed metal species are being pursued.

Supplementary material

CCDC 952479-952485 contain the supporting crystallographic data for **1–7**, which can be obtained free of charge from the Cambridge Crystallographic Data Center, 12 Union Road, Cambridge CB2 1EZ, UK; Fax: (44) 01223-336033; E-mail: deposit@ccdc.cam.ac.uk or via http://www.ccdc.cam.ac.uk/conts/retrieving.html.

Acknowledgements

This work was supported by the Laboratory Directed Research and Development (LDRD) program at Sandia National Laboratories. The Bruker X-ray diffractometer used for some crystal solutions was purchased via a National Science Foundation CRIF:MU award to the University of New Mexico (CHE04-43580). Sandia is a multiprogram laboratory operated by Sandia Corporation, a Lockheed Martin Company, for the United States Department of Energy's National Nuclear Security Administration under Contract DE-AC04-94AL85000.

References

[1] D.C. Bradley, R.C. Mehrotra, I.P. Rothwell, A. Singh. *Alkoxo and Aryloxo Derivatives of Metals*, Academic Press, San Diego, CA (2001).
[2] D.C. Bradley, R.C. Mehrotra, D.P. Gaul. *Metal Alkoxides*, Academic Press, New York (1978).
[3] D.C. Bradley. *Chem. Rev.*, **89**, 1317 (1989).
[4] C.D. Chandler, C. Roger, M.J. Hampden-Smith. *Chem. Rev.*, **93**, 1205 (1993).
[5] K.G. Caulton, L.G. Hubert-Pfalzgraf. *Chem. Rev.*, **90**, 969 (1990).
[6] M.Y. Turova, E.P. Turevskaya, V.G. Kessler, M.I. Yanovskaya. *The Chemistry of Metal Alkoxides*, Kluwer Academic Publishers, Boston, MA (2002).
[7] T.J. Boyle, L.A.M. Steele, D.T. Yonemoto. *J. Coord. Chem.*, **65**, 487 (2012).
[8] T.J. Boyle, L.A.M. Ottley. *Inorg. Chim. Acta*, **364**, 69 (2010).
[9] V.G. Kessler, G.I. Spijksma, G.A. Seisenbaeva, S. Håkansson, D.H.A. Blank, H.J.M. Bouwmeester. *J. Sol-Gel Sci. Technol.*, **40**, 163 (2006).
[10] Conquest (Version 1.15), Cambridge Crystallographic Data Centre: support@ccdc.cam.ac.uk or http://www.ccdc.cam.ac.uk [CSD Version 5.34, November (2012)].
[11] T.J. Boyle, T.M. Alam, E.R. Mechenbier, B.L. Scott, J.W. Ziller. *Inorg. Chem.*, **36**, 3293 (1997).
[12] T.J. Boyle, L.A.M. Ottley, S.M. Hoppe. *Inorg. Chem.*, **49**, 10798 (2010).
[13] Z. Skrzat. *Acta Cryst. Sect. B*, **B36**, 2812 (1980).
[14] Z. Skrzat. *Acta Cryst. Sect. B*, **B36**, 3201 (1980).
[15] Z. Skrzat, A. Konitz. *Pol. J. Chem.*, **54**, 1029 (1980).

[16] K. Chaitanya, C. Santhamma, K.V. Prasad, V. Veeraiah. *J. At. Mol. Sci.*, **3**, 1 (2012).
[17] A. Zhang, J. Zhang, Q. Pan, S. Wang, H. Jia, B. Xu. *J. Lumin.*, **132**, 965 (2012).
[18] P.A. Srinivasan, M. Suganthi. *Asian J. Chem.*, **20**, 1775 (2008).
[19] T.J. Boyle, L.A.M. Ottley, M.A. Rodriguez. *Polyhedron*, **24**, 1727 (2005).
[20] T.J. Boyle, R.P. Tyner, T.M. Alam, B.L. Scott, J.W. Ziller, B.G. Potter. *J. Am. Chem. Soc.*, **121**, 12104 (1999).
[21] T.J. Boyle, T.M. Alam, C.J. Tafoya, B.L. Scott. *Inorg. Chem.*, **37**, 5588 (1998).
[22] N. Pajot, R. Papiernik, L.G. Hubert-Pfalzgraf, J. Vaissermann, S. Parraud. *Chem. Commun.*, 1817 (1995).
[23] P. Piszczek, M. Richert, A. Grodzicki, T. Głowiak, A. Wojtczak. *Polyhedron*, **24**, 663 (2005).
[24] P.S. Ammala, S.R. Batten, C.M. Kepert, L. Spiccia, A.M. van den Bergen, B.O. West. *Inorg. Chim. Acta*, **353**, 75 (2003).
[25] F.R. Kogler, M. Jupa, M. Puchberger, U. Schubert. *J. Mater. Chem.*, **14**, 3133 (2004).
[26] G. Kickelbick, P. Wiede, U. Schubert. *Inorg. Chim. Acta*, **284**, 1 (1999).
[27] S. Gross, G. Kickelbick, M. Puchberger, U. Schubert. *Monatsh. Chem.*, **134**, 1053 (2003).
[28] M. Puchberger, F.R. Kogler, M. Jupa, S. Gross, H. Fric, G. Kickelbick, U. Schubert. *Eur. J. Inorg. Chem.*, **16**, 3283 (2006).
[29] R.D. Shannon. *Acta Cryst.*, **A32**, 751 (1976).